FÖLL
priv. copy

13

phys. stat. sol. (a) **49**, 555 (1978)

Subject classification: 1.4 and 10

Institut für Physik, Max-Planck-Institut für Metallforschung, Stuttgart

The Black–White Vector $\boldsymbol{l}$ of Small Dislocation Loops on Transmission Electron Microscope Images

By

M. WILKENS and H. FÖLL[1])

Starting from the analytical approximation of the black–white contrast figures of small dislocation loops a simple analytical expression is derived for the angle φ_l between the black–white vector $\boldsymbol{l}$ and the diffraction vector $\boldsymbol{g}$ for dynamical two-beam conditions. It is shown that φ_l depends essentially only on the direction of a vector $\boldsymbol{m}$ (= "mean orientation vector") which bisects the acute angle between the Burgers vector $\boldsymbol{b}$ and the plane normal $\boldsymbol{n}$ of the dislocation loop. The influence of the shear angle ε (= acute angle between $\boldsymbol{b}$ and $\boldsymbol{n}$) on φ_l is in general negligible.

Ausgehend von der analytischen Näherungslösung der Schwarz–Weiß-Kontraste kleiner Versetzungsringe wird ein analytischer Ausdruck abgeleitet für den Winkel φ_l zwischen dem Schwarz–Weiß-Vektor $\boldsymbol{l}$ und dem Beugungs-Vektor $\boldsymbol{g}$ im dynamischen Zweistrahlfall. Es wird gezeigt, daß φ_l im wesentlichen durch die Richtung eines Vektors $\boldsymbol{m}$ (= „mittlerer Orientierungs-Vektor") bestimmt wird, wobei $\boldsymbol{m}$ den spitzen Winkel zwischen Burgers-Vektor $\boldsymbol{b}$ und Ebenennormale $\boldsymbol{n}$ des Versetzungsringes teilt. Der Einfluß des Scherwinkels ε (spitzer Winkel zwischen $\boldsymbol{b}$ und $\boldsymbol{n}$) auf φ_l ist im allgemeinen zu vernachlässigen.

1. Introduction

Dislocation loops which are too small to be resolved as loops on transmission electron microscope images can be analysed in terms of their crystallographic parameters (Burgers vector $\boldsymbol{b}$, normal vector $\boldsymbol{n}$ of the loop plane) by means of the black–white (BW) contrast method [1 to 6]. In the first papers concerning this subject [7, 8] it was assumed that the direction of the so-called BW vector $\boldsymbol{l}$ (pointing from the centre of the main dark lobe to the centre of the main bright lobe of a BW contrast figure) is parallel to the direction of $\boldsymbol{b}_{\text{pr}}$ where $\boldsymbol{b}_{\text{pr}}$ is the projection of the Burgers vector $\boldsymbol{b}$ of the loop onto the image plane, i.e. the plane of the micrograph. Later it was recognized by an inspection of computer-calculated two-dimensional BW contrast figures of pure edge loops in elastically isotropic crystals that this assumption is not correct [5]: If φ_l and φ_b are the acute angles in the image plane between the diffraction vector $\boldsymbol{g}$ and $\boldsymbol{l}$ and between $\boldsymbol{g}$ and $\boldsymbol{b}_{\text{pr}}$, respectively, it turned out that in the cases considered in [5] the ratio φ_l/φ_b was in general only 0.6 to 0.7 instead of unity. Further, considering the BW contrast of loops with shear components ($\boldsymbol{b}$ inclined to the loop plane) Rühle and Wilkens [9] could not find any simple relation between φ_l and φ_b.

In the meantime an analytical first-order perturbation solution was derived [4], describing the BW contrast of small dislocation loops. This first-order perturbation solution is in particular suitable for a fast calculation of the constant-intensity contour diagrams in the "outer regions" of a BW contrast figure.[2])

[1]) Present address: Department of Materials Science and Engineering, Cornell University, Ithaca, N.Y., USA.

[2]) A BW contrast figure may be subdivided into the "inner region" (diameter of the order of the loop diameter) and the "outer region". The present paper is concerned with the contrast in the outer region. Special features of the BW contrast in the inner region which are useful for the determination of $\boldsymbol{b}$ are discussed by Eyre et al. [5, 6] and Katerbau [10].

The analytical solution has proved to be very useful for a detailed analysis of the directions of $\boldsymbol{b}$ and $\boldsymbol{n}$ of the dislocation loop responsible for the BW contrast. This is done by comparison of the characteristics of the shapes of experimentally observed and theoretically predicted contrast figures without making use of the concept of BW vector $\boldsymbol{l}$, cf., e.g., [11, 12]. On the other hand, the angle φ_l as introduced above can be measured fairly easily on experimentally obtained BW contrast figures. Therefore, it appears worthwhile to investigate theoretically the dependence of the angle φ_l as a function of the directions of $\boldsymbol{n}$ and $\boldsymbol{b}$. This is the subject of the present paper.

2. Characterization of Loop Orientations: The Mean Orientation Vector $\boldsymbol{m}$

We use a Cartesian coordinate system with the origin in the upper specimen surface through which the electrons penetrate into the specimen (z-axis parallel to the electron beam, x-axis parallel to the diffraction vector $\boldsymbol{g}$). Within the image plane (x–y plane) we also use polar coordinates ϱ and φ,

$$\varrho^2 = x^2 + y^2 , \qquad \tan \varphi = \frac{y}{x}, \tag{2.1}$$

with $\varrho = 0$ at the image position of the loop centre.

In addition to the normal $\boldsymbol{n}$ of the loop plane and the Burgers vector $\boldsymbol{b}$ of the loop we introduce a "mean orientation vector" $\boldsymbol{m}$ which bisects the acute angle between $\boldsymbol{n}$ and $\boldsymbol{b}$,

$$\boldsymbol{m} = \frac{\boldsymbol{n} \pm \boldsymbol{\beta}}{|\boldsymbol{n} \pm \boldsymbol{\beta}|} \tag{2.2}$$

with $\boldsymbol{\beta} = \boldsymbol{b}/|\boldsymbol{b}|$. The upper (lower) sign holds for loops of vacancy type characterized by $\boldsymbol{n} \cdot \boldsymbol{b} > 0$ (interstitial type; $\boldsymbol{n} \cdot \boldsymbol{b} < 0$), cf. [4].

We denote the unit vectors $\boldsymbol{n}$, $\boldsymbol{\beta}$, and $\boldsymbol{m}$ either by their direction cosines, i.e., we write them in the form

$$\boldsymbol{v} = (v_x, v_y, v_z) , \tag{2.3}$$

where $\boldsymbol{v}$ stands for $\boldsymbol{n}$, $\boldsymbol{\beta}$ or $\boldsymbol{m}$, respectively, or by the acute angle between $\boldsymbol{g}$ and the projection of $\boldsymbol{v}$ onto the image plane, $\varphi_{\boldsymbol{v}}$, and the angle between $\boldsymbol{v}$ and the image plane, $\alpha_{\boldsymbol{v}}$. The following relation then holds:

$$\tan \varphi_{\boldsymbol{v}} = \frac{v_y}{v_x} , \qquad \sin \alpha_{\boldsymbol{v}} = v_z . \tag{2.4}$$

A non-edge loop ("loop with shear component") is described by the "shear angle" ε between $\boldsymbol{n}$ and $\boldsymbol{\beta}$ such that

$$\cos \varepsilon = |\boldsymbol{n} \cdot \boldsymbol{\beta}| . \tag{2.5}$$

In the following we consider for non-edge loops two extreme cases concerning the mutual orientation of $\boldsymbol{n}$ and $\boldsymbol{\beta}$, cf. Fig. 1:

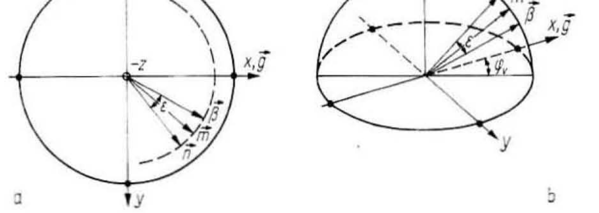

Fig. 1. Stereographic projections of the unit vectors $\boldsymbol{n}$ and $\boldsymbol{\beta}$ for non-edge loops. a) Case A, equation (2.6); b) case B, equation (2.7)

$$\text{Case A} \qquad \beta_z = \pm n_z \tag{2.6}$$

with + (−) for loops of vacancy (interstitial) type.

$$\text{Case B} \qquad \left.\begin{aligned} \varphi_{\boldsymbol{\beta}} &= \varphi_{\boldsymbol{n}} && \text{vacancy type ,} \\ &= \varphi_{\boldsymbol{n}} + \pi && \text{interstitial type .} \end{aligned}\right\} \tag{2.7}$$

3. Constant-Intensity Contour Diagrams

The analytical representation of the constant-intensity contour diagrams of BW contrast figures of small dislocation loops in elastically isotropic crystals [4] may be written in the form

$$\varrho = \frac{C}{\Delta I} F(\varphi) , \tag{3.1}$$

where ΔI is the relative deviation from the background intensity. The term C, which will not be considered here in detail, oscillates in sign and magnitude with the depth position z_0 of the loop centre in the foil, i.e. C describes the structure of the so-called layers of depth oscillations [1, 4, 8]. In the following we assume that the loop centre are located well within these layers, i.e. sufficiently apart from their borders. If this is not the case the structure of the BW contrast figure is more complicated (Rühle [13], cf. also [4, 6]). The angular function $F(\varphi)$ is given by

$$F(\varphi) = F^{(1)}(\varphi) + qF^{(2)}(\varphi) , \tag{3.2}$$

$$= a_1 \cos \varphi + a_3 \cos 3\varphi + b_1 \sin \varphi + b_3 \sin 3\varphi \tag{3.3}$$

with

$$a_n = a_n^{(1)} + qa_n^{(2)} , \qquad b_n = b_n^{(1)} + qb_n^{(2)} . \tag{3.4}$$

The coefficients $a_n^{(i)}$, $b_n^{(i)}$ ($i = 1, 2$) are functions of Poisson's ratio ν and depend bilinearly on the direction cosines of $\boldsymbol{n}$ and $\boldsymbol{\beta}$, cf. [4]. The term q is of the order of unity and depends weakly on ϱ. We neglect this ϱ-dependence and set

$$q = 1 \tag{3.5}$$

throughout this paper.[3]) Under this condition the coefficients a_n, b_n take the form as given in the Appendix.

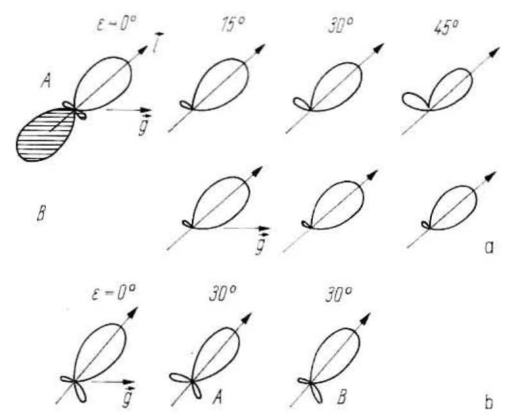

Fig. 2. Constant-intensity contour diagrams (as calculated by means of (3.1) with $|C/\Delta I| = 1$ and $\nu = \frac{1}{3}$) for non-edge loops having the same mean orientation vector $\boldsymbol{m}$ but different shear angles ε. The dark and the bright lobes are shown in one case only. In the other cases the dark lobes (which are always centro-symmetric to the bright lobes) are omitted, for simplicity. A and B refer to (2.6) and (2.7), respectively. The BW vector $\boldsymbol{l}$ drawn through the lobes are calculated by means of (4.2). a) $\varphi_{\boldsymbol{m}} = 60°$, $\alpha_{\boldsymbol{m}} = 30°$; b) $\varphi_{\boldsymbol{m}} = 75°$, $\alpha_{\boldsymbol{m}} = 0°$

[3]) In [4] the function $F(\varphi)$ was approximated by $F(\varphi) \approx 1.5F^{(1)}(\varphi)$ because $F^{(2)}(\varphi) \approx 0.5F^{(1)}(\varphi)$ holds in many cases. Föll [14] has shown that this approximation may give rise to inconsistent results. This is true in particular if the criterion $a_1^{(2)}/a_1^{(1)} \gtrapprox -0.5$ for the visibility of a BW contrast figure as proposed in [4] is applied to cases where ν is small and $\boldsymbol{n}$ and $\boldsymbol{b}$ are close to the y-axis.

We have applied (3.1) to a number of non-edge loops having the same mean orientation vector $\boldsymbol{m}$. Fig. 2 contains some representative examples referring to $\nu = \frac{1}{3}$. It is found that the directions and strengths of the main lobes (black or white) are hardly affected by $\varepsilon \neq 0$.

In the case A (equation (2.6)) there is some minor influence of ε on the strength of the subsidiary lobes which becomes noticeable, however, only for $\varepsilon \gtrapprox 30°$ (for the classification into „main" and „subsidiary" lobes see [3, 4]). In the case B (equation (2.7)) this influence is negligible.

In this context it is worthwhile to mention that, in general, the strength of the subsidiary lobes increase with decreasing ν. Therefore, a comparison of experimental BW contrast figures with calculated constant-intensity contour diagrams should be done with an appropriate choice of ν inserted into the coefficients of (3.4).

4. Direction of the BW Vector $\boldsymbol{l}$

Equation (3.1) indicates that the strength of the term $F(\varphi)$ is a measure of the strength of the contrast along the direction given by the angle φ. This suggests the following representation of the acute angle φ_l between $\boldsymbol{g}$ and $\boldsymbol{l}$:

$$\frac{\partial}{\partial \hat{\varphi}} \int_0^{2\pi} F^2(\varphi) \cos^2 (\varphi - \hat{\varphi}) \, d\varphi = 0 \quad \text{for } \hat{\varphi} = \varphi_l \text{ or } \varphi_l + \pi. \tag{4.1}$$

This definition means we rotate a test function $\cos^2 (\varphi - \hat{\varphi})$ (the square of the simplest BW contrast figure) over the function $F^2(\varphi)$ and take the angle $\hat{\varphi}$ where maximal coverage of the two functions is obtained as φ_l. Therefore, in (4.1) the angle φ_l is essentially determined by the angular positions of the centres of gravity of the main lobes. Subsidiary lobes, if they occur, have only minor influence on the determinative of φ_l. This corresponds best to the experimental procedure by which φ_l is measured.

With (3.3) inserted into (4.1) we obtain after some algebraic operations

$$\tan 2\varphi_l = 2 \frac{a_1(b_1 + b_3) - a_3 b_1}{a_1^2 - b_1^2 + 2a_1 a_3 + 2b_1 b_3}. \tag{4.2}$$

The vectors $\boldsymbol{l}$ inserted in the constant-intensity contour diagrams in Fig. 2 were calculated by means of this equation. Obviously, $\boldsymbol{l}$ coincides well with the black–white vector one would determine experimentally.

In Fig. 3 we have plotted the ratio

$$R = \frac{\varphi_l}{\varphi_m} \tag{4.3}$$

as a function of φ_m for pure edge loops with α_m and ν as parameters. The curves $R = R(\varphi_m)$ are terminated near $\varphi_m \approx 75°$. Around and beyond this value the BW

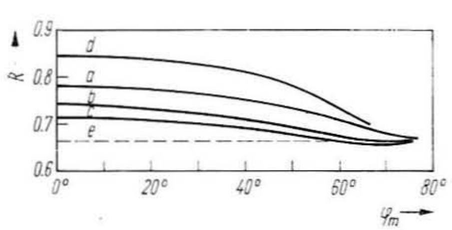

Fig. 3. The ratio $R = \varphi_l/\varphi_m$ for pure edge loops as a function of φ_m. (a) $\alpha_m = 0°$, $\nu = 1/4$; (b) $\alpha_m = 0°$, $\nu = 1/3$; (c) $\alpha_m = 0°$, $\nu = 2/5$; (d) $\alpha_m = 45°$, $\nu = 1/4$; (e) $R = 2/3$, cf. (5.3)

contrast figures become so "strongly distorted" (cf. [3, 4]) that a BW vector $\boldsymbol{l}$ can no longer be defined.

From the results the following conclusions can be drawn:

(i) The ratio R takes its maximum value for $\varphi_m = 0$ and decreases with increasing φ_m. For a given value of φ_m the ratio R increases with decreasing ν and with increasing α_m. However, for the range of the values of α_m and ν considered, R approaches to about the same value $R = 0.67 \pm 0.01$ for φ_m approaching 70°.

(ii) Comparing pure edge loops and non-edge loops of the same direction of $\boldsymbol{m}$ it is found that φ_l varies by less than 1° in the interval $\varepsilon \lessapprox 45°$. This holds for the two extreme cases of non-edge loops as indicated by (2.6) and (2.7) (cf. also Fig. 1) and also for intermediate cases. Thus the curves in Fig. 3 calculated originally for pure edge loops are applicable also for non-edge loops.

5. Discussion

In the general case the orientation of a dislocation loop with respect to the diffraction vector $\boldsymbol{g}$ and the direction of the electron beam is characterized by four parameters, e.g., by the angles φ_n, α_n, φ_β, and α_β. Therefore, a representative investigation of the value of φ_l as a function of these four parameters and of Poisson's ratio ν is fairly tedious if solely computer-calculated two-dimensional contrast figures are used. However, the problem is easily solved by (4.2) derived in the present paper.

One striking result of our calculations is that the shape of the outer region of a BW contrast figure and, hence, the angle φ_l is to a good degree determined only by the parameters φ_m and α_m which characterize the mean orientation vector $\boldsymbol{m}$. This facilitates the calculations further.

In order to understand the result reported in the preceding paragraph we refer to the fact that in the first-order perturbation solution [4], which is applied in the present paper, the displacement field of a small dislocation loop is represented by that of elastic double forces located at the loop centre. This approximation, which has proved to be very good for the outer region of a BW contrast figure, has the consequence that the displacement field and, hence, the contrast figure remains unchanged if the directions of $\boldsymbol{n}$ and $\boldsymbol{b}$ are interchanged ("$\boldsymbol{n}$–$\boldsymbol{b}$ symmetry").[4]

Since the constant-intensity contour diagrams (CICD) are analytic functions of the direction cosines of $\boldsymbol{g}$ and $\boldsymbol{\beta}$ and, hence, of ε, it follows from the $\boldsymbol{n}$–$\boldsymbol{b}$ symmetry that — comparing loops of the same direction of $\boldsymbol{m}$ — the CICD are independent of ε in *linear* approximation. This explains the weak influence of ε on the shapes of the CICD and, in particular, on the angle φ_l.

Another analytical representation of φ_l was recently published by Ohr [16]. His approach is based on the same first-order perturbation solution [4] as used in the present paper but defines φ_l instead of (4.1) by

$$\frac{\partial F(\varphi)}{\partial \varphi} = 0 \quad \text{for} \quad \varphi = \varphi_l . \tag{5.1}$$

Ohr's expression is so far worked out only for $\boldsymbol{n}$ and $\boldsymbol{b}$ within the image plane and for a particular value of ν (presumably $\nu = \frac{1}{3}$). Further, it represents φ_l by an implicit equation only, in contrast to (4.2) of the present paper. For practical application the solution of such an implicit equation is inconvenient. Further, one may argue that

[4]) Recent remarks published in the literature (Holmes et al. [15], Eyre et al. [6]) which state that this $\boldsymbol{n}$–$\boldsymbol{b}$ symmetry is not fulfilled are not correct and are obviously based on a misunderstanding of the arguments given in [4]. Of course, the $\boldsymbol{n}$–$\boldsymbol{b}$ symmetry may not be valid for the "inner region" of the contrast figure where the displacement field of a loop with finite diameter must be used for the contrast calculations.

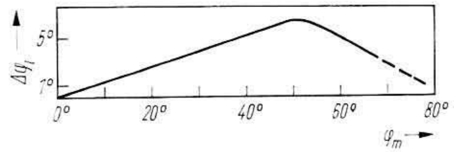

Fig. 4. The systematic variation $\Delta\varphi_l$ defined in (5.2) as a function of φ_m

for the experimental determination of φ_l the directions of the maxima of the main lobes, on which the definition of φ_l in (5.1) is based, are less significant than the centres of gravity of the main lobes which are relevant for our representation, cf. Section 4.

Ohr's paper is mainly concerned with φ_l as a function φ_n and φ_β. A variation of the parameters α_m, ε, and ν was not considered explicitly. With the formula given in Section 4 this is easily done and we proceed as follows: We denote by $\pm\delta\varphi_l$ the *experimental* uncertainty which is associated to φ_l as measured on a micrograph. As an estimate we set $\delta\varphi_l = 2°$. In Section 4 it was stated that within this estimate the variation of φ_l as a function of ε can be neglected. With respect to a *systematic* variation of φ_l as a function of α_m and ν we refer to the two extreme cases (c) and (d) in Fig. 3 ((c): $\alpha_m = 0°$, $\nu = 0.4$; (d): $\alpha_m = 45°$, $\nu = 0.25$). Using these two cases we define a maximum systematic variation $\Delta\varphi_l$ by

$$\Delta\varphi_l = \varphi_m(R_{(d)} - R_{(c)})\,. \tag{5.2}$$

In Fig. 4 we have plotted $\Delta\varphi_l$ as a function of φ_m. The result is that $\Delta\varphi_l \lessapprox 2\delta\varphi_l$ ($\approx 4°$) for $\varphi_m \lessapprox 30°$ and $\varphi_m \gtrapprox 65°$. However, for φ_m around 45° the value of $\Delta\varphi_l$ may be slightly larger than 6°. This means that in this region of φ_m the systematic variation of φ_l may exceed the experimental uncertainty.

In [16] a "rule of thumb",

$$\varphi_l \approx \frac{2}{3}\varphi_m\,, \tag{5.3}$$

was proposed which is represented in Fig. 3 as case (e) (dashed line). Obviously this case is close to case (c) of Fig. 3. Consequently (5.3) represents in general a lower limit of φ_l and is a reasonable approximation if only a moderate accuracy in the calculation of φ_l is attempted. If, however, the systematic uncertainties should be kept as small as possible, then the explicit representation of φ_l in (4.2) may be a significantly better approach than (5.3).

In a preceding paper (Föll and Wilkens [17]) which was concerned with the separate determination of the directions of $\boldsymbol{n}$ and $\boldsymbol{b}$ of small dislocation loops in heavy-ion damaged hexagonal cobalt we have shown that (4.2) gives reasonable results which are self-consistent when the same kind of loops were imaged by different two-beam diffraction vectors $\boldsymbol{g}$ and different crystallographic directions of the incident electron beam.

6. Conclusions

Starting from an analytical expression for the constant-intensity contour diagrams (CICD) of the black–white contrast figure of small dislocation loops the following results were obtained:

(i) For the purpose of the CICD calculations a given non-edge loop (loop with shear component) can be replaced in good approximation by a fictitious pure edge loop with the loop normal $\boldsymbol{n}$ being equal to the mean orientation vector $\boldsymbol{m}$ of the respective non-edge loop.

(ii) A simple explicit formula is derived for the angle φ_l between the black–white vector $\boldsymbol{l}$ and the diffraction vector $\boldsymbol{g}$ which holds for dislocation loops without and with shear components. For the latter case it is shown that φ_l can be calculated in very good approximation assuming a fictitious dislocation loop of pure edge type as indicated in (i).

Appendix

With equations (3.4) and (3.5) and [4] we obtain

$$a_1 = \left(\frac{13}{2} - 4\nu\right) n_x\beta_x - \left(\frac{1}{2} - 4\nu\right) n_y\beta_y - (2 - 4\nu)\, n_z\beta_z\,,$$

$$a_3 = \frac{3}{2}(n_x\beta_x - n_y\beta_y)\,,$$

$$b_1 = \left(\frac{7}{2} - 4\nu\right)(n_x\beta_y + n_y\beta_x)\,, \qquad b_3 = \frac{3}{2}(n_x\beta_y + n_y\beta_x)\,.$$

Acknowledgement

The authors are indepted to Dr. M. Rühle for valuable critical comments during the preparation of the manuscript.

References

[1] M. Rühle, phys. stat. sol. **19**, 263 (1967).
[2] M. Wilkens, in: Modern Diffraction and Imaging Techniques in Materials Science, Ed. S. Amelinckx, R. Gevers, R. Remaut, and J. van Landuyt, North-Holland Publ. Co., Amsterdam 1970 (p. 233).
[3] M. Wilkens, in: Electron Microscopy in Materials Science, Vol. II, Ed. U. Valdrè and E. Ruedl, Commission of the European Communities, Luxemburg 1976, (p. 647).
[4] M. Wilkens and M. Rühle, phys. stat. sol. (b) **49**, 749 (1972).
[5] B. L. Eyre, in: Defects in Refractory Metals, Ed. R. de Batist, J. Nihoul, and L. Stals, S.C.K./C.E.N., Mol, 1971 (p. 311).
[6] B. L. Eyre, D. M. Maher, and R. C. Perrin, J. Phys. F **7**, 1359 (1977).
[7] U. Essmann and M. Wilkens, phys. stat. sol. **4**, K53 (1964).
[8] M. Rühle, M. Wilkens, and U. Essmann, phys. stat. sol. **11**, 819 (1965).
[9] M. Rühle and M. Wilkens, Proc. VII. Internat. Conf. Electron Microscopy, Vol. II, Grenoble 1970, (p. 311).
[10] K.-H. Katerbau, phys. stat. sol. (a) **38**, 463 (1976).
[11] F. Häussermann, M. Rühle, and M. Wilkens, phys. stat. sol. (b) **50**, 445 (1972).
[12] W. Jäger and M. Wilkens, phys. stat. sol. (a) **32**, 89 (1975).
[13] M. Rühle, phys. stat. sol. **19**, 279 (1967).
[14] H. Föll, Diploma Work, Stuttgart 1973 and unpublished results.
[15] S. M. Holmes, B. L. Eyre, and R. C. Perrin, Proc. VI. European Congr. Electron Microscopy, Vol. I, Jerusalem 1976, (p. 279).
[16] S. M. Ohr, phys. stat. sol. (a) **38**, 553 (1976).
[17] H. Föll and M. Wilkens, phys. stat. sol. (a) **39**, 561 (1977).

(Received June 26, 1978)